FOI-R–0173–SE
October 2001
ISSN 1650-1942

Scientific report

Momme Butenschön

Numerical Analysis of Time Dependent External Disturbances on Separated Axisymmetric Nozzle Flow

Master Thesis

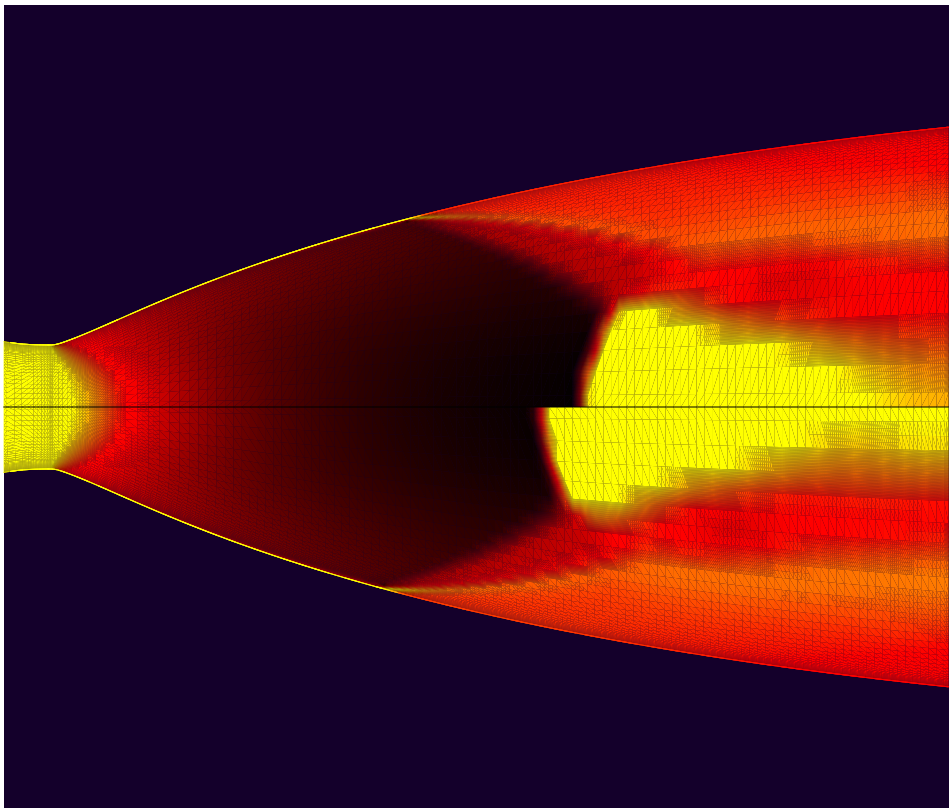

Division of Aeronautics, FFA
SE-172 90 STOCKHOLM

FOI – Swedish Defence Research Agency
Division of Aeronautics, FFA
SE-172 90 STOCKHOLM

FOI-R–0173–SE
October 2001
ISSN 1650-1942

Scientific report

Momme Butenschön

Numerical Analysis of Time Dependent External Disturbances on Separated Axisymmetric Nozzle Flow

Master Thesis

Division of Aeronautics, FFA
SE-172 90 STOCKHOLM

Abstract

In overexpanded rocket nozzle flow at low altitudes, the sensitivity of the shock structure, that develops inside the expansion part of the nozzle, causes severe problems in modern nozzle design. This shock structure is highly unstable, so that small fluctuations in the flow field can lead to heavy asymmetric loads on the nozzle. The movement of the shock structure is analyzed numerically by imposing a periodically fluctuating pressure to an external boundary face. The effects on the sideloads are estimated by an usteady axisymmetric analysis. The unsteady analysis shows, for the investigated frequency range, how the fluctuation propagates, the shock movement develops and sideloads are generated.

Contents

1 Introduction

The greatest challenge in supersonic nozzle design nowadays is to create a nozzle with a reasonably good performance at sea level conditions, corresponding to low pressure ratios between the nozzle's combustion chamber and the environment, without loosing performance at high altitudes at its nominal pressure ratio. There exists a variety of newer and older ideas how to design such a nozzle as eg. the plug-nozzle or the dual-bell-nozzle (see [8]), but in the end they all suffer from the fact that the type of flow that occurs at sea level conditions, is so far, not very well understood.

Figure 1. Ariane launch (picture from ESA).

As the nozzles nominally expand to a level below the ambient pressure, the flow has to recompress in some way. It achieves that by establishing a shock structure in the expanding part of the nozzle, that separates the flow from the wall and concentrates it in the center of the nozzle bounded by a supersonic jet, while on the nozzle wall recirculation pockets form, that suck air from the environment into the nozzle.

The behavior of this flow structure is very sensitive to fluctuations in the flow, and thus, might become highly unsteady and asymmetric. Also hysteresis effects appear, as the structures for identical conditions vary depending on if the flow originated from higher or lower pressure ratios than the actual state. The main problem of this phenomenon lies in the fact, that small fluctuations can create very heavy side loads, which not only affect the lateral stability of the nozzle's driving force, but also can lead to severe damage in the nozzle material (compare [4]).

Thus, it is of utmost interest to study and understand the physical mechanisms that create these sideloads, in order to be able to design a nozzle where the inner shock structure is controlled.

The driving mechanism behind those sideloads is most of all the angular asymmetry of the strength and position of the shock attached to the nozzle wall. Therefore, the sensitivity of this shock to changes in pressure is essential for this asymmetry to develop. It is the aim of this work

to contribute to a better understanding of the effect of fluctuating pressure on shock structure and sideloads. To achieve that, steady and unsteady computations were performed, examining the inner flow field of a supersonic nozzle, with special emphasis of the shock on the nozzle wall. In the steady computations a pressure ratio was determined which provided an appropriate shock position. The obtained solutions were tested with regard to the mesh convergence, turbulence modeling and some numerical variations. After that the set-up for the unsteady computations was defined. A periodically fluctuating pressure was applied to the boundary at the nozzle exit, using different frequencies to illuminate the shock's capability of reaction.The following analysis covers eg. the general flow field, the propagation of the fluctuations into the nozzle and the resulting sideloads. Due to the restricted extent of this project all computations were performed as axisymmetric.

2 The Generation of the Numerical Model

The modeling of a complex flow structure like that of a nozzle is quite a delicate process. A lot of approximations and simplifications have to be done in abstracting the flow case to a mathematical and then a numerical model. This will always include a compromise between complexity and accuracy. It is the art of the engineer to decide by careful selection and intuition which models that will be most suitable to achieve the aims of his actual work.

2.1 The Reduction of a 3-dimensional Flow to an Axisymmetric Model

Overexpanded flow through a supersonic nozzle involves clearly three dimensional effects, and especially the generation of sideloads is an expression of purely asymmetric effects. Thus, it might seem meaningless to analyze this type of flow on the base of an axisymmetric model. How should a symmetric model be able to describe an asymmetric behavior?

If the differences of the flow between planes in radial directions of the nozzle are regarded as variations of a mean solution over these radial intersections, then a comparison between single intersections can provide an approximation of unsteady effects. If these intersections are assumed to be decoupled, they can be given by axisymmetric solutions, which should describe the direct influence of pressure fluctuations that approach the inner nozzle's shock structure in axial direction quite well.

However, the reduction to an axisymmetric case has its weaknesses. Effects of secondary flows in radial or circumferential direction can not be described and the interaction between the radial intersections is completely neglected. Moreover, the most unstable dynamic modes of the shock structure movement might not be axisymmetric and, thus, such modes cannot be captured in an axisymmetric analysis.

Nevertheless, this work presents a purely axisymmetric analysis, which still allows an investigation of the sensitivity of the shock structure and gives an estimate of some of the modes that generate sideloads. However, for a complete and quantitative correct description, a fully three-dimensional model would be indisputable. The axisymmetric approximation reduces considerably the numerical effort in performance as well as in preparation and a full 3D analysis is out of the scope for this work.

2.2 The Mesh and the Boundary Conditions

One of the first problems tackled in building a model to investigate a physical phenomenon is the question, where to put the boundaries of the computational domain, depending on the purpose of the model. As this investigation focuses on the structure of the flow inside the nozzle, in the

beginning only the inner part of the nozzle was considered to reduce the computational effort. Moreover, for the unsteady analysis a direct coupling between the prescribed pressure and the pressure un the nozzle was desirable. Only at the nozzles inlet a short section of constant diameter was added to guarantee uniform inflow (see also Lindblad & Butenschön [11]). The expanding part of the nozzle is supplied with a rather dense distribution of points over a wide area, as the shock is expected to move considerably through this region inside the nozzle.

The mesh is based on the geometry of the truncated ideal contour version of the s6-nozzle, developed by the Volvo Aero Corporation, a subscaled version of the Vulcain nozzle [3]. Three different resolutions were extracted, a coarse one having 4 000 points, the medium one with about 16 000 points and the fine one with about 64 000 points.

Figure 2. The first mesh in medium resolution.

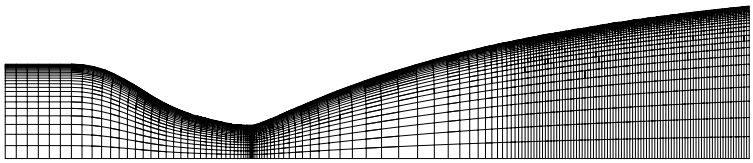

The boundaries are defined as

- subsonic inflow at the nozzle inlet, stagnation conditions and flow direction are imposed, static pressure is extrapolated from the interior
- no slip wall for the nozzle wall
- singular line for the nozzle symmetry axis
- mirror conditions on the circumferential faces
- at the exit Riemann invariants are used, allowing inflow and outflow in different regions of the same boundary face

Unfortunately, the exit condition was not able to establish a supersonic jet while having inflow into the recirculation pockets on the nozzle wall. Instead, the flow is slowed down to a subsonic level directly in front of the nozzle exit, as can be seen in figure 3. The picture clearly shows, how the supersonic jet is forced to a subsonic speed before leaving the nozzle. This effect is present through the range of all computed pressure ratios and independent of the mesh resolution and the applied numerical methods. It is clearly an effect of the chosen boundary condition, which can be confirmed by an analysis of its theory:

The Riemann invariants are defined as

$$R_+ = v_n + \frac{2a}{\gamma - 1} \qquad R_- = v_n - \frac{2a}{\gamma - 1} \quad , \qquad (1)$$

Figure 3. The slowdown effect of the exit condition. Mach number at the pressure ratio of 16.

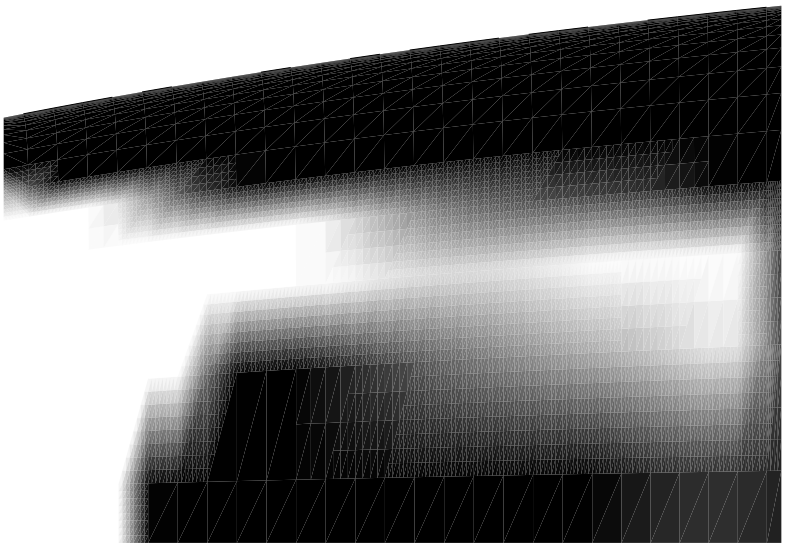

where v_n is the normal velocity component pointing into the control volume, a is the local speed of sound and γ is the ratio of the specific heats. These invariants are taken from the inside or outside of the control volume depending on the flow direction and if it is supersonic or subsonic. The invariants outside of the control volume are determined from the specified boundary condition. For subsonic in- and outflow, this would be

$$R_+ = v_{n,\infty} + \frac{2a_\infty}{\gamma - 1} \qquad R_- = v_{n,i} - \frac{2a_i}{\gamma - 1} \tag{2}$$

and therefore, the values on the boundary become

$$v_n = \frac{v_{n,\infty} + v_{n,i}}{2} + \frac{a_\infty - a_i}{\gamma - 1} \quad , \tag{3}$$

$$a = \frac{v_{n,\infty} - v_{n,i}}{4}(\gamma - 1) + \frac{a_\infty + a_i}{2} \quad , \tag{4}$$

where the index i denotes the values in the first cell inside the boundary, while the index ∞ refers to the specified freestream condition outside of the boundary.

At the outlet boundary of the nozzle flow of this work the subsonic core of the flow is enclosed in a supersonic ring, which itself is surrounded by the recirculation region on the wall with a shear layer in between.

We want to estimate now, under which conditions recirculation and subsonic outflow can form from a situation with subsonic outflow over the outlet boundary. In case of recirculation, v_n and $v_{n,i}$ will be greater than zero and for a nozzle flow we can state that at least for outflow and for the numerical transition from outflow to subsonic inflow the freestream will be colder than the flow inside the nozzle. From 3 we can derive

$$\frac{v_{n,\infty} + v_{n,i}}{2} > \frac{1}{\gamma - 1}(a_i - a_\infty) \quad . \tag{5}$$

The right hand side is positive, thus the left hand side must at least be positive as well, which yields

$$|v_{n,\infty}| < |v_{n,i}| \tag{6}$$

as a necessary condition for the formation of a recirculation area at the nozzle exit. The prescribed Mach number must, thus, be close to zero.

We consider now a location on the boundary, where the flow is directed out of the system. With equations 3 and 4, we can form the normal Mach number

$$M = 5\frac{5a_i - v_{n,i} - 5a_\infty - v_{n,\infty}}{5a_i - v_{n,i} + 5a_\infty + v_{n,\infty}} \quad . \tag{7}$$

(with $\gamma = 1.4$, mind that $v_{n,i}, v_{n,\infty}, v_n < 0$!)

We can express that in terms of the Mach numbers and substitute $\Delta a = (a_i - a_\infty)/a_\infty$:

$$M = 5\frac{(1 + \Delta a)M_i + 5\Delta a + M_\infty}{(1 + \Delta a)M_i + 5\Delta a - M_\infty + 10} \quad , \tag{8}$$

where now all quantities are positive.

To achieve supersonic outflow, we need $M > 1$. Thus, we obtain

$$2M_i + 2\Delta a M_i + 3M_\infty + 10\Delta a > 5 \tag{9}$$

Following equation 6 we have to choose M_∞ close to zero, if we want to establish a recirculation area on the boundary face, which yields

$$\Delta a > \frac{5 - 2M_i}{10 + 2M_i} \tag{10}$$

as a relation between the inner Mach number and the change of the sound velocity over the boundary or

$$T_i > \left(\frac{15}{10 + 2M_i}\right)^2 T_\infty \tag{11}$$

in terms of temperature change and inner Mach number. In the numerical transition process towards a supersonic outflow, the inner Mach number cannot be much larger than 1. That infers, that the temperature just inside the boundary has to be 1.6 times higher than the freestream temperature, which can barely be achieved here.

We conclude, that a boundary condition based on Riemann invariants will fail to establish a supersonic jet and a recirculation into the system using the same freestream conditions.

A way to avoid this problem would be, to give the freestream values as a field, but, doing so, one would define parts of the exit face to be supersonic and others to be subsonic and by this control the formation of the whole flow structure behind the shock instead of letting it develop freely. However, the size of the compression-expansion pattern behind the shock has also a significant influence on the shock at the wall itself and the sideloads, as mentioned by Romine [16]. Thus, the Riemann-field condition was not regarded as a favorable set-up for this case.

Instead of this, an extra block was included, adding an area downstream of the nozzle exit of about twice the nozzle length with a lateral boundary following the wall contour with an inclination of $6.0°$ with respect to the nozzle centerline, allowing the flow to develop freely through the nozzle exit (see figure 4).

At the downstream exit of the system the flow can now be extrapolated, as it is now certainly directed out of the control volume, while it is computed from Riemann invariants at the lateral face, which does not yield a problem anymore, as the complete face is now subsonic. The freestream values used for the computation of the Riemann invariants were chosen close to static atmospheric conditions with just a small velocity in the main flow direction to initiate the flow in the right direction. For the complete set of boundary conditions see table 1.

It is important to mention that the extra part was not designed to give an exact picture of the flow through this part, but to support a physically correct picture inside the nozzle. This is also the reason, why this part is largely excluded in the discussion of the results. The sizes of the new set of meshes are given in table 3. All meshes for this project were generated using FFANET [17].

2.3 Modeling Methods

Supersonic nozzle flow is naturally of a highly compressible and turbulent character. For this work its physics are modeled using the Reynolds averaged Navier-Stokes (RANS) equations, as implemented in the structured finite-volume solver for compressible flow EURANUS [15]. These equations have to be closed by some sort of turbulence-model. A variety of algebraic, two equational and algebraic Reynolds Stress models is

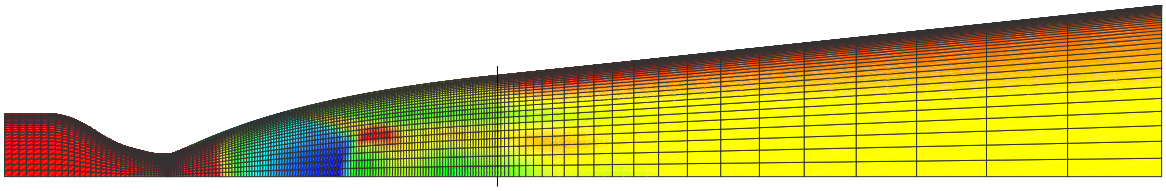

Figure 4. The extended mesh in medium resolution overlaid on the density field at pressure ratio 16.

Table 1. The boundary conditions for the extended mesh.

block	face	boundary condition
1	imin	inflow*
1	imax	matching
1	jmin	singular line
1	jmax	no slip wall
1	kmin	mirror
1	kmax	mirror
2	imin	matching
2	imax	0-order extrapolation
2	jmin	singular line
2	jmax	Riemann invariants*
2	kmin	mirror
2	kmax	mirror

*see table2

available in the code of EURANUS, for this case mainly two models were chosen:

- the Menter SST model [12], a two-equational model based on a blending between a k-ω and a k-ϵ formulation that uses the Boussinesq hypothesis [1], including also a production limiter
- the explicit algebraic Reynolds stress model (EARSM) introduced by Wallin & Johansson [18], that uses an anisotropic approach for the turbulent stresses, combined with Menter's BSL model [12], a version of the SST model without limiter

Table 2. The flow conditions.

	p[bar]	T[K]	$u\left[\frac{\mathrm{m}}{\mathrm{s}}\right]$	$v\left[\frac{\mathrm{m}}{\mathrm{s}}\right]$	$w\left[\frac{\mathrm{m}}{\mathrm{s}}\right]$
inflow	6-24	500	1	0	0
freestream	1	288	1	0	0

Table 3. The dimensions of the extended mesh.

	nozzle			extra block		
resolution	i	j	k	i	j	k
coarse	80	25	2	13	25	2
medium	159	49	2	25	49	2
fine	317	97	2	49	97	2

Spatial discretization is accomplished by

- either a 2nd order central scheme or a 2nd order TVD upwind scheme with Van Leer limiters [10] for the mean flow equations
- a 2nd order symmetric TVD upwind scheme with Van Leer limiters [10] for the turbulence equations

Computations showed better convergence with the central scheme for the mean equations, while there were no significant differences in the physical results, thus this combination was preferred. An entropy fix is applied for the upwind scheme to avoid unphysical solutions.

For the unsteady computations time is advanced using implicit integration with pseudo-time relaxation [9, 5], for the steady computations time is advanced using a 5-stage Runge Kutta scheme.

Furthermore, multigrid computations were tested, but did not converge, so that time consuming singlegrid computations are used instead.

The gas in the nozzle is assumed to be air and since the temperature is quite modest, it is modeled as a calorically perfect gas with a ratio of the specific heats of $\gamma = 1.4$ and the gas constant $R = 287.0$ J/kg K. For the molecular viscosity Sutherland's law is used.

3 Steady State Analysis

A number of computations were performed for the steady case with a number of different numerical set-ups. They were started on the coarse mesh at a pressure ratio of 6 between the combustion chamber and the environment, where the shock structure is located shortly behind the throat of the nozzle. Then the chamber pressure was raised step by step until the shock structure almost reached the nozzle exit (see figure 7). In the region of interest investigations on mesh convergence, turbulence modeling and numerical schemes were intensified. The general flow structure revealed by these computations was principally the same and corresponded to the observations of other authors, eg. [14, 2, 6].

3.1 The Flow Structure

At overexpanding conditions, while the flow follows the nozzle contour, it expands to a pressure level that is far lower than the ambient pressure. As it is supersonic it cannot adapt gradually, but is suddenly forced by a shock to adapt to the ambient conditions. This strong shock in the nozzle center is almost normal and usually referred to as the Mach disk (see figure 5). In addition to that an oblique shock separates the boundary layer from the

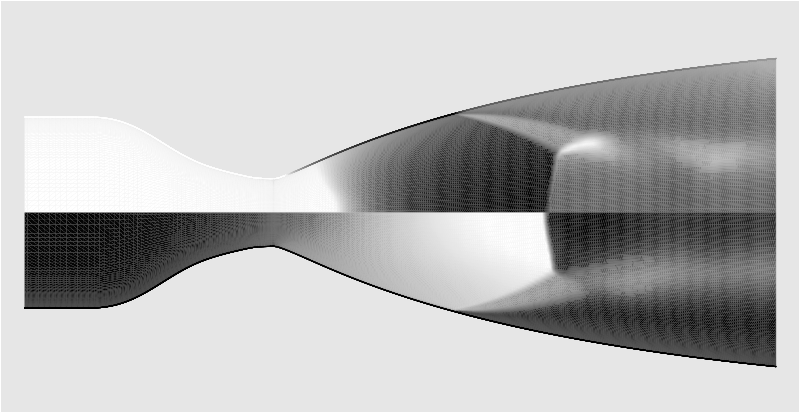

Figure 5. The flow structure at pressure ratio 16, medium mesh, SST model. Top: density. Bottom: Mach number.

wall and deflects the flow towards the nozzle center. A small third shock appears where the two shocks meet. It redirects the streamlines into the main flow direction. Air is flowing from the ambience into the nozzle at the wall and a recirculation area develops as it is driven along with the jet (figure 6).

The recompressed jet in the nozzle center does not expand with the wall contour anymore, but takes the width that is adequate for the present pressure conditions. It is subsonic in the center behind the Mach disk, but the stream deflected by the oblique shock remains supersonic and encloses the subsonic core. A shear layer establishes between the jet and the recirculation area.

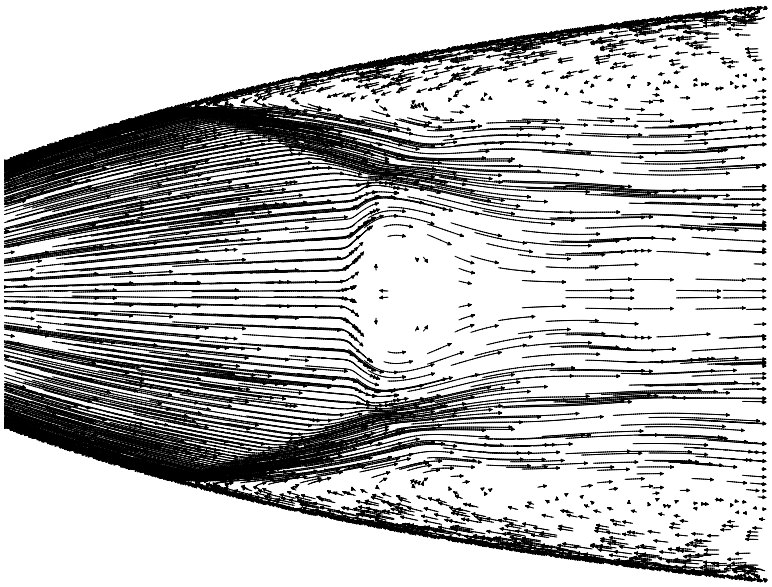

Figure 6. The velocity field at pressure ratio 16, medium mesh, SST model.

For some nozzles the flow will reattach to the wall at higher pressure ratios enclosing a recirculation bubble. The shift between the two flow patterns occurs abruptly and not simultaneously on the whole circumference of the nozzle, which generates large unpredictable sideloads to the nozzle. Those effects were reported by eg. Frey & Hagemann [7] and Onofri & Nasuti [13]. However, the nozzle selected for this work does not show this phenomenon, and was chosen because the shock movement is not distorted or restricted by these effects. Only, if the shock movement under free conditions is understood, one will be able to control it, so that also a controlled change from one pattern to the other becomes possible.

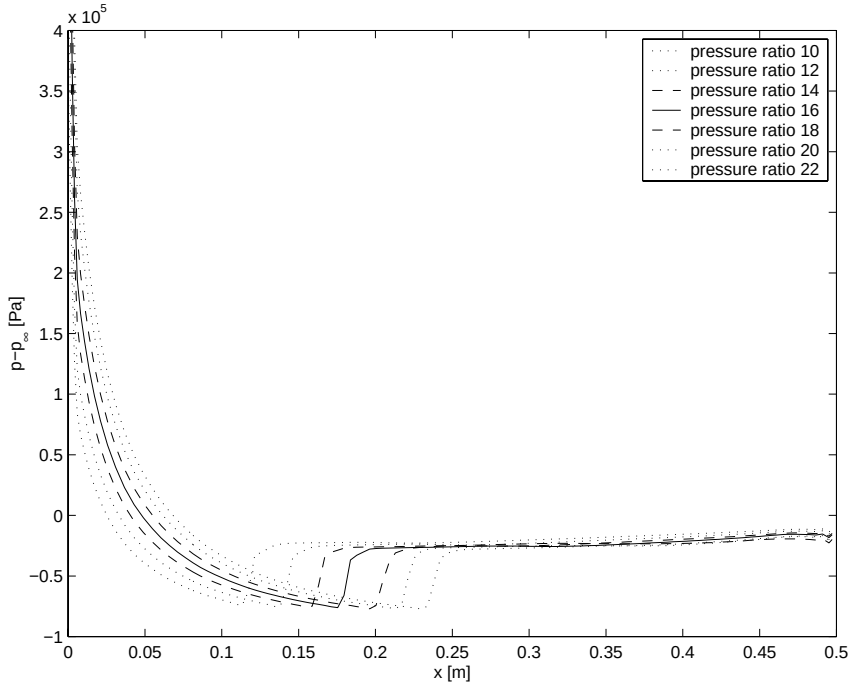

Figure 7. The wall pressure at different pressure ratios, medium mesh, SST model.

The general character of the flow field for this nozzle does not change with varying pressure ratio, even if the shock moves considerably downstream while increasing the chamber pressure, as figure 7 shows. One difference in the flow field is, that the Mach disk becomes more and more convex with higher pressure ratios, which indicates the growth of the vortex just behind the Mach disk (see figure 6).

The existence of this vortex is a curiosity in the numerical analysis of overexpanded nozzle flow. It does not appear in all solutions, but was observed in reattached flow (eg. [13, 6]) as well as in free separated flow (eg. [13]) and in the plume (eg. [6, 2]). Though the shock structure of numerical solutions with core vortex provided by some authors corresponds to flow pictures from experiments, the existence of the vortex was never directly confirmed. It seems that the vortex formation in the computations is connected to a convex bending of the Mach disk, that occurs with rising pressure ratio. In this case only the computations on the pressure ratios of 6 and 8 showed a concave Mach disk without core vortex, for all higher ratios the Mach disk is convex and a vortex appears.

Nevertheless, the shock movement seems to be quite regular in the regarded region, moving with about the same distance for each pressure step.

A detailed analysis of a nozzle flow field, that also contains considerations of start up and throttle down process is given by Chen et al. [2], Frey and Hagemann [6] provide an overview of the flow patterns that occur in supersonic nozzles including the nozzle downstream region.

3.2 Mesh Convergence

For all three mesh resolutions, computations were performed for several pressure ratios to obtain a reliable picture of the mesh convergence. The computations took about 20 000 to 25 000 iterations to converge for the coarse and the medium mesh, while for the finest mesh 10 000 iterations were sufficient. The computation at each grid level was initiated by the coarser grid solution. In all cases the iterative process was continued to a higher number of iterations, but it neither reduced the residuals any further nor showed a change in the flow field of the solutions.

Figure 8 shows, that the solution for the coarse mesh differs significantly from the other two meshes. The flow starts separating 10 % of the nozzle length further downstream than for the other two meshes. Though this resolution shows generally the same flow structure, it resolves the shock pattern obviously not sufficiently to generate a solution that is consistent with the other two meshes.

However, the medium and the fine mesh show a quite good agreement of the overall flow field. The position of the Mach disk is slightly different, as the medium mesh cannot provide the same sharp picture of the thickness of the shock here, which induces differences in the Mach number in the jet core, see figure 9. Nevertheless, the supersonic part of the jet and especially the situation at the wall match almost perfectly in both structure

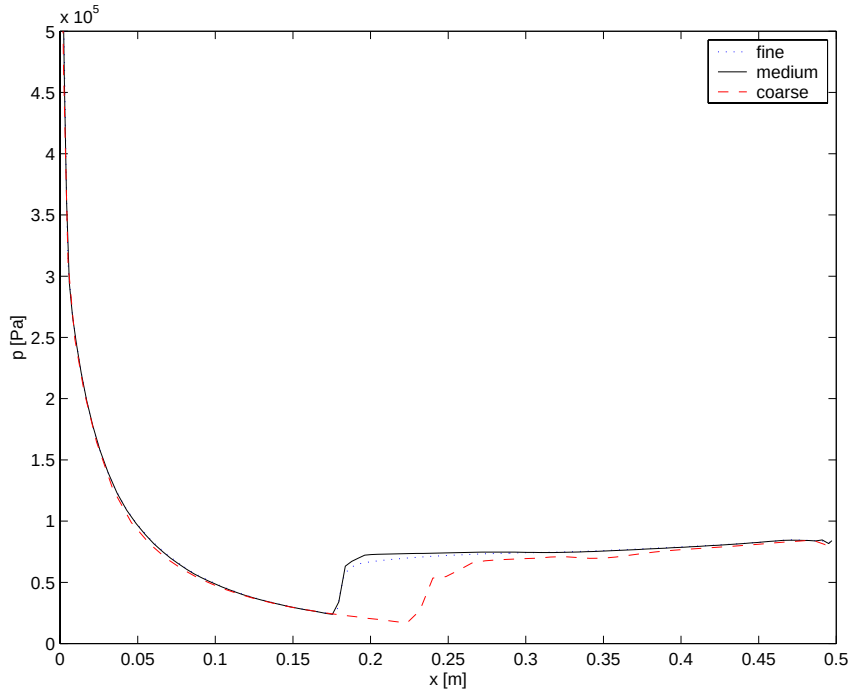

Figure 8. The wall pressure for three different mesh resolutions, pressure ratio 16, SST model.

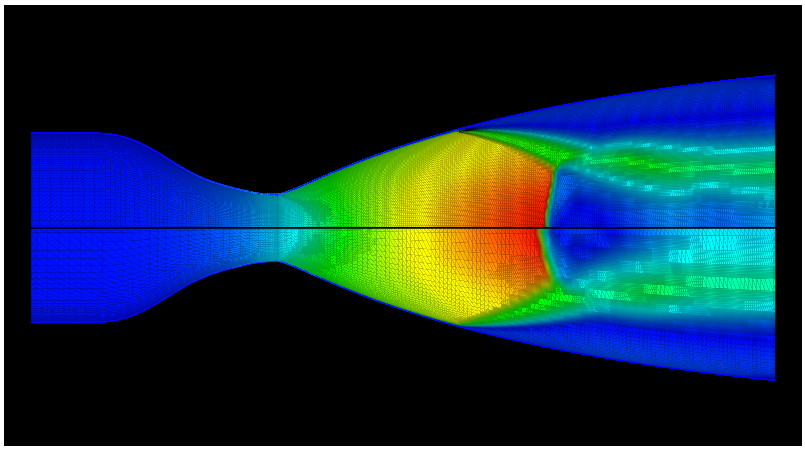

Figure 9. Mach number at pressure ratio = 16, SST model. Top: fine mesh. Bottom: medium mesh model.

and magnitude.

It can be concluded, that a grid converged solution for this set-up is found, and that the medium mesh is sufficient for a correct picture of the main flow structure and the wall pressure.

3.3 Turbulence Models

For a complex flow like this one with shock induced boundary layer separation, recirculation, free shear layer, strong shock, shock reflection, slipstream and strong vorticity it is obvious that only an advanced turbulence model will provide the necessary tool to obtain reliable solutions as a base for this analysis. Simple models, such as algebraic, one equational or standard two equational models, will fail to predict these structures reasonably. On the other hand, a rather complex model, that includes transport equa-

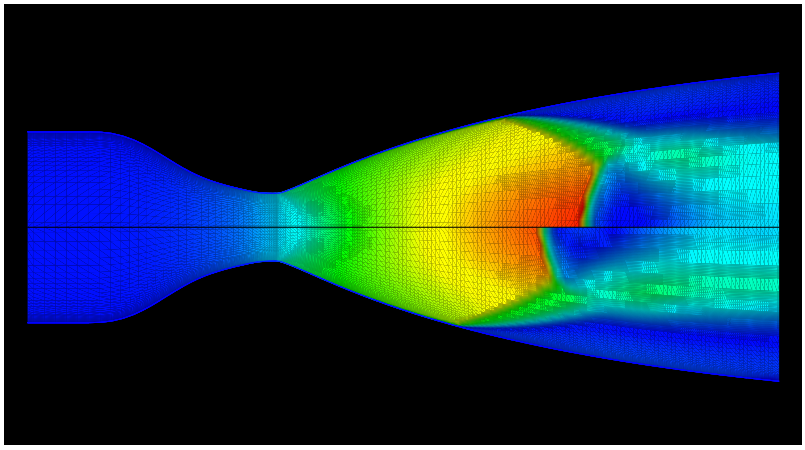

Figure 10. Mach number at pressure ratio 16, medium mesh. Top: EARSM model. Bottom: SST model.

tions for higher statistical moments of the turbulent fluctuations, would not only demand a much higher amount of computational power for a case, that at least in the unsteady part is already with a simple model approaching the limits for a project like this one, but would also involve additional numerical problems, as the transport equations of these moments are highly nonlinear and stiff. Other approaches, such as Large eddy simulation (LES) or direct numerical simulation (DNS), that do not use the RANS-equations, are for the moment and in the near future for this case beyond the capabilities of modern computers. Thus, this case requires a model that is reliable in predicting even the critical elements in turbulence modeling, but at the same time numerically simple, stable and fast.

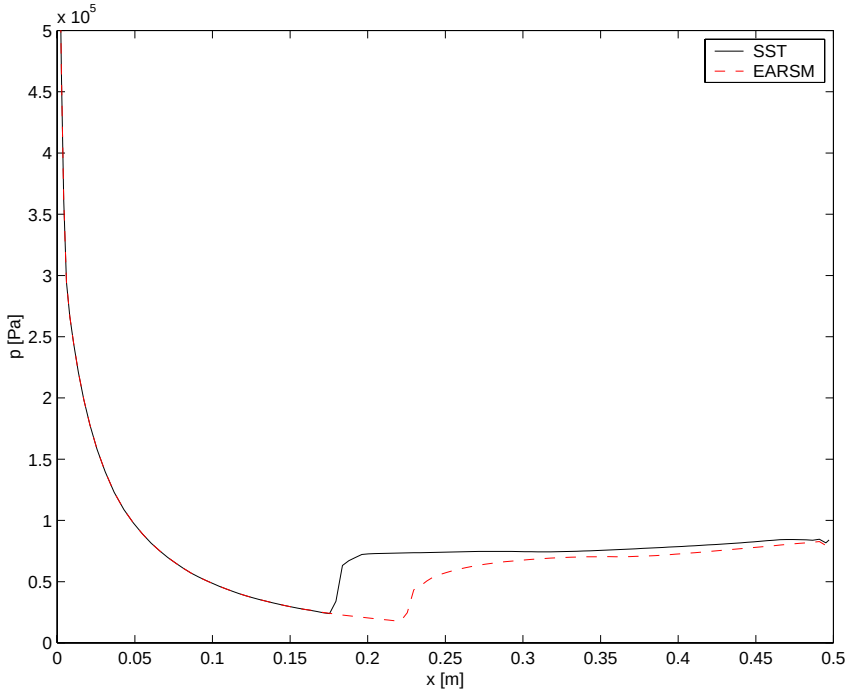

Figure 11. The wall pressure for different turbulence models, pressure ratio 16.

Two models were chosen out of the long list of turbulence models currently available. The Menter SST model [12], that showed robust behavior and quite good results in other nozzle computations using the same code

[14, 11] and the EARSM of Walling & Johanson [18], that performed well on a variety of other test cases, also using EURANUS (see eg. [18]). The Wilcox standard k-ω model [20] with a production limiter was also tested, but showed severe problems in establishing any solution at all.

The flow fields for the two computed models do have the same features, but the whole shock structure is shifted 10 % of the nozzle length and differs in magnitude (figure 10). Even though the EARSM expands further than the SST model, the oblique shock is weaker and its shape is less well defined, as shown in figure 11. This might be due to the higher turbulent viscosity in the recirculation region (figure 12). Also the viscosity produced by the center vortex behind the Mach disk is much higher for the EARSM.

Both models have a high level of turbulent kinetic energy in the shear layer, even if the SST model again produces little less, but behind the Mach disk the EARSM develops a huge amount, while the SST model just shows a very weak increase in turbulent energy.

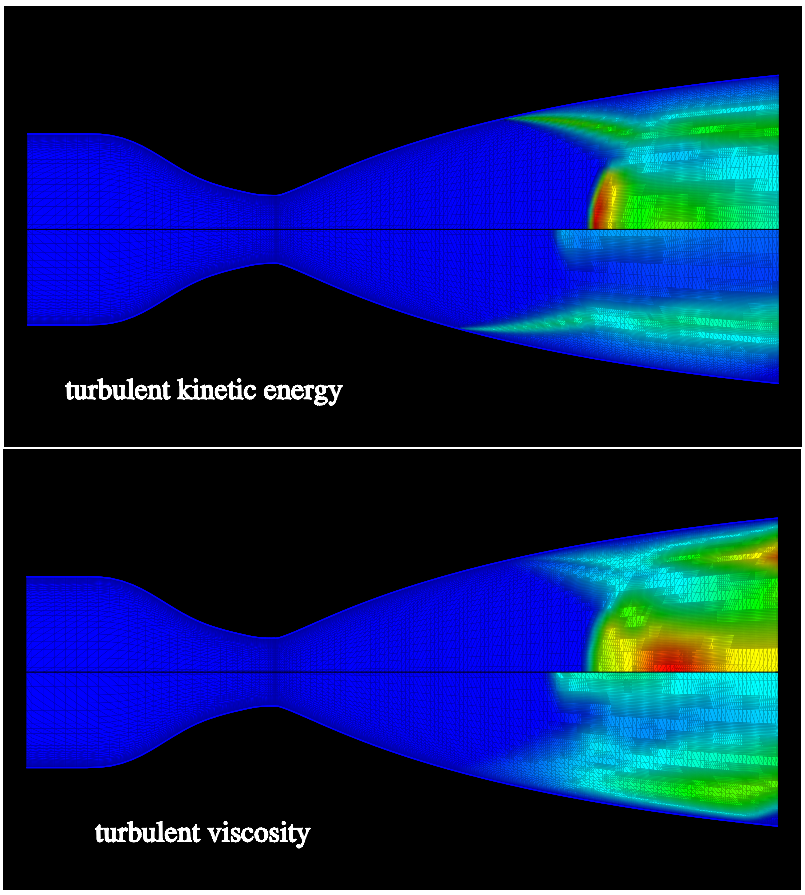

Figure 12. Turbulent kinetic energy and turbulent viscosity at pressure ratio = 16, medium mesh. Top: EARSM model. Bottom: SST model.

The generally higher level of turbulence for the EARSM is probably the reason for the later separation of the flow. As the losses in the jet are considerably higher than for the SST model, the maximum speed inside the nozzle has to be higher to assure the same conditions, when the jet exhausts to the ambience. Also, the high turbulence level behind the Mach disk has

a damping effect on the recirculation area, so that the oblique shock can separate further downstream.

The question remains, if the high level of turbulence produced by the EARSM compared to the SST model induced by the strong shock is a general feature of these models or significant for this case. Moreover, the highly complex shock structure could make the numerical treatment of the turbulent models important. It is, however, not obvious which of these two solutions is closest to reality.

4 Unsteady Analysis

Starting from a steady solution the movement of the shock was excited by pressure fluctuations that were enforced on the lateral face of the block downstream of the nozzle exit. Different frequencies were applied to examine the capability of the shock to react on fast changes in pressure and the effect of this on the sideloads.

4.1 The Unsteady Boundary Condition

To be able to impose the fluctuating pressure on the lateral face the EURANUS code [15] had to be extended with a time dependent Riemann boundary condition. This condition evaluates the flow state on the boundary from the freestream condition given by the user and the interior of the flow. The fluctuation was defined in form of a harmonic perturbation of 10 % amplitude of the mean freestream pressure. This fluctuation was assumed to spread with sound velocity in the non-moving ambience. A fluctuating pressure must consequently induce a change in the other state variables. For the sake of consistency, the perfect gas law was applied for these changes and two assumptions were considered for this case: an isothermal change of state and an isentropic change of state in the freestream, where the isothermal change has the advantage of a constant sound velocity. The Riemann invariants were given in equation 1 as

$$R_+ = v_n + \frac{2a}{\gamma - 1} \qquad R_- = v_n - \frac{2a}{\gamma - 1} \quad .$$

This provides two equations for the normal velocity component and two state variables, thus, one more equation is needed. The assumption, that the change of the variables across the boundary is isentropic, yields

$$\frac{p}{\rho^\gamma} = const \quad . \tag{12}$$

Using these three equations the relation between the imposed freestream pressure and the pressure on the boundary can be derived. It is

$$p_{BC} \sim p_{free}(t) \tag{13}$$

for the isothermal freestream or

$$p_{BC} \sim \left(c_1 p_{free}^{\frac{\gamma-1}{2\gamma}}(t) + c_2 \right)^{\frac{2\gamma}{\gamma-1}} \tag{14}$$

for the isentropic freestream. Both boundary conditions approach identities between p_{BC} and p_{free} when the difference between freestream and interior vanishes and thus, can be considered consistent.

Mind that in the total iteration process those relations are not as explicit as it might seem, as the factors in equation 13 and 14 depend on the interior

of the flow field. Nevertheless, it is obvious, that the relation between $p_{free}(t)$ and p_{BC} is more direct for the isothermal case.

For the above reasons the isothermal condition seems to be advantageous for this case and was therefore used throughout the whole analysis. Nevertheless, a solution for isentropic conditions was compared to the isothermal. It didn't show any major differences in the inner flow field of the nozzle, but showed a slightly slower convergence.

Apart from this face the same boundary conditions were used as in the steady case, as given in tables 1 and 2.

4.2 Definition of the Flow Case

Out of the number of steady solutions one case was chosen as reference case for the unsteady analysis. It was used for comparison of the results, but also as an initial solution for the time marching computations.

4.2.1 The Reference Case

The main criterion in selecting a reference case was to find the pressure ratio that provides a suitable position of the shock with regard to the respective turbulence model and mesh resolution. As the flow fields showed no significant differences between the medium mesh and the fine mesh, and especially since the situation at the wall is well described, the medium mesh was regarded to be sufficiently resolved. The SST turbulence model was chosen, as it gives a sharper picture of the shock at the wall. Also, it was shown in [14], that already the SST model tends to predict the shock further downstream, than it occurred in experiments, so that the EARSM solution might be expected to give an even larger deviation (see figure 11). However, those computations were performed on a different nozzle.

Table 4. The reference case.

$p_{chamber}$[bar]	p_∞[bar]	mesh	turbulence model
16	1 ± 10 %	medium	SST

Given the turbulence model and the resolution, a pressure ratio had to be determined, that would place the shock structure in a favorable position, i.e. far enough downstream of the throat region, but not too close to the exit to minimize interactions with the plume. Figures 4 and 14 show that for the ratio of 16 the shock structure is located quite well within the nozzle, which completes the definition of the reference case. It is summarized in table 4.

4.2.2 Time Step and Inner Iterations

Another important part is the choice of the time step and the number of inner iterations. Wang et al. [19] showed, that an increased number of time

steps does not necessarily lead to a higher number of total iterations, as the iterative process per time step converges faster. However, these results were obtained on another flow case, and it is not sure that this constellation will show the same behavior.

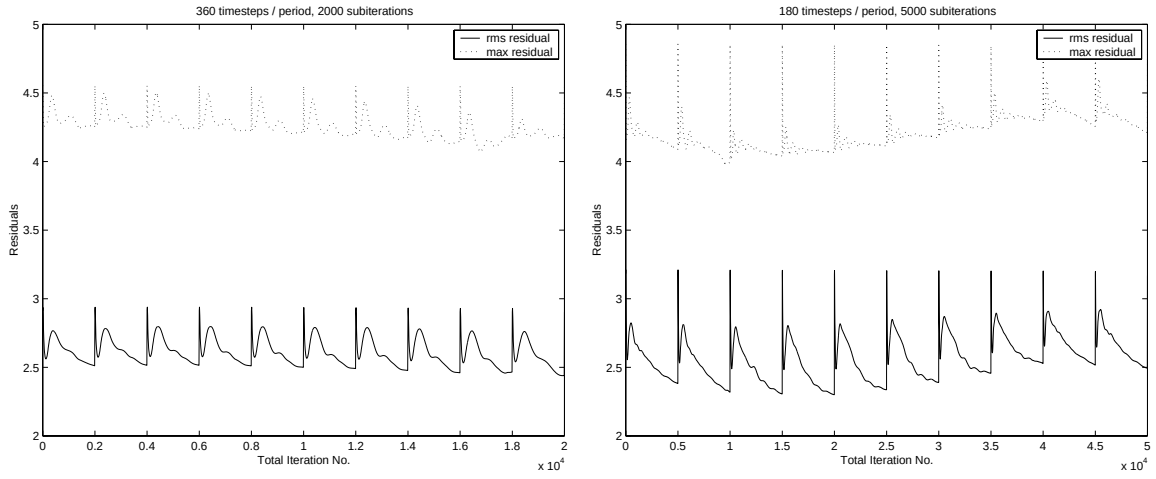

Figure 13. Iterative Process.

In figure 13 the first ten global time steps in one period of the pressure fluctuation are compared for two different set-ups for the time step and the subiteration number. It can be seen that the maximum deflection at the beginning of the time step is half as big for the smaller time step with 360 steps per period, while the general course of the iterative process per time step is the same for both resolutions in time. Thus, the shape of the

Figure 14. Three evaluation points with Mach number field at pressure ratio 16, SST model, medium mesh.

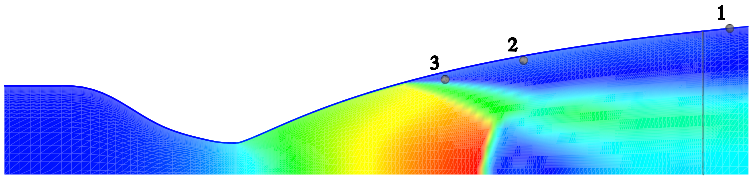

iterative behavior of the solutions does not seem to change with the size of the global time step. Nevertheless, for the finer resolution in time the solution process bends towards a converged state at little less then 2000 subiterations, while the solution with 180 time steps per period seems not to have fully converged at 5000 iterations, which implies a faster convergence towards the final state. In figure 15 the pressure evolution in time is demonstrated in three different points, that are visualized in figure 14. It shows that there appear no considerable differences anymore in the physical magnitudes of the flow field. Also the solution with 4000 iterations for the smaller time step does not differ significantly. Thus, the set-up with a resolution of 360 time steps per period and 2000 subiterations was chosen for the analysis.

The small oscillations that appear at the two inner points are discussed in section 4.3.

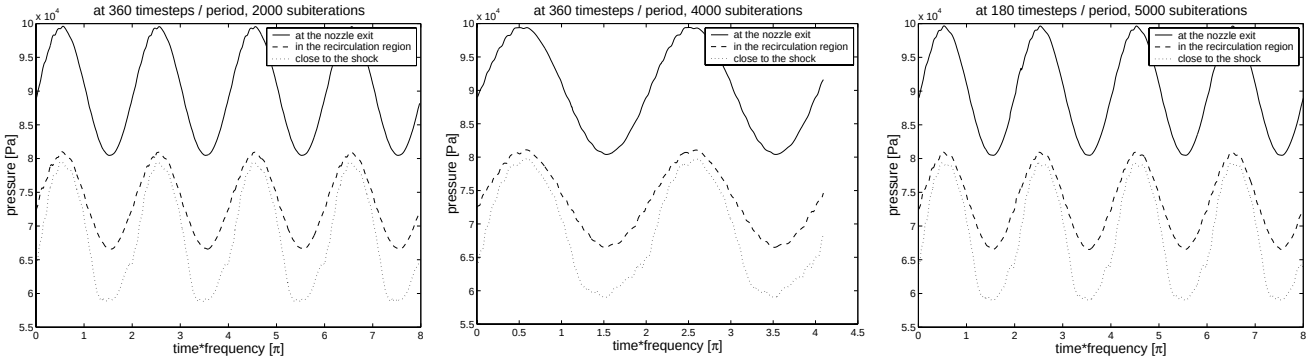

Figure 15. The pressure history for different iterative set-ups.

4.2.3 The Imposed Fluctuation

On the flow conditions of the reference case a fluctuating pressure was imposed on the external lateral face to excite the shock movement away from the steady state solution. The fluctuation has sinus-form and an amplitude of 10 % of the ambient pressure of the reference case, which corresponds to a movement of the shock on the nozzle wall of 0.018 m in direction of the nozzle axis, estimated from the steady solutions (figure 7).

The most precarious choice for this case is probably the set of the frequencies chosen for the analysis. The sideloads, that act on the nozzle will be strongly influenced by the frequency of the fluctuations. For low frequencies the pressure acting on the nozzle wall will be rather constant, while for faster fluctuations the pressure varies considerably along the nozzles wall. Then, if the frequency gets very high, the fluctuations on the wall get so dense, that they can be considered constant again. A possibility to obtain a quantitative estimation of a reasonable choice of frequencies is to determine a wavelength $\lambda = 2\pi a_\infty/\omega$ of the fluctuations corresponding to a propagation with the sound velocity a_∞ of the freestream and compare it to the nozzle length L. The computations in this work were started with a fluctuation wavelength of $30L$, to achieve a slow changing flow that could be considered as quasi steady. The second frequency of $\omega = 1000$ s^{-1} corresponds to a wavelength of $4L$. At a third frequency of $\omega = 1500$ s^{-1} the pressure fluctuates with a third of a period over one nozzle length, so that a full amplitude of fluctuation covers a nozzle length and a change in the behavior of the sideloads is encouraged. The frequency was increased quite carefully, as the reaction of the oblique shock on the wall on the frequencies is expected to add changes to the sideload's behavior.

In addition to that a fourth frequency was tested as the velocity field at the unsteady boundary showed some unexpected behavior. Figure 16

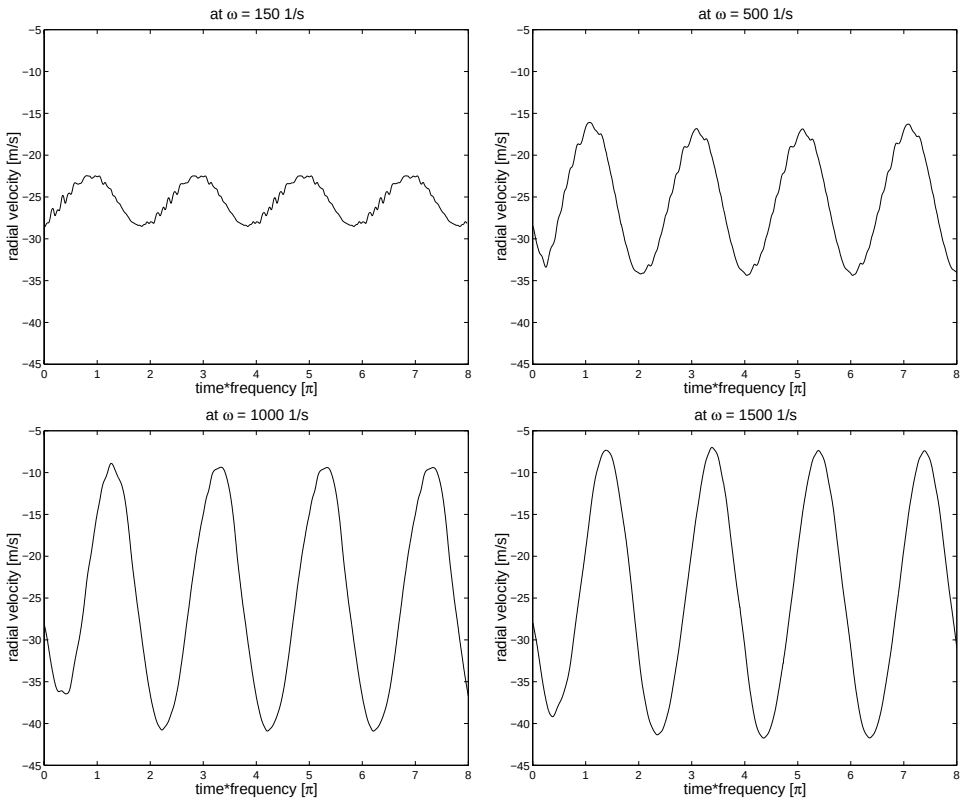

Figure 16. The radial velocity at the unsteady boundary close to the nozzle exit at 360 timesteps per period, 2000 subiterations.

shows that there is a perturbation of a higher frequency overlaid on the fluctuation of $150\ \mathrm{s}^{-1}$. Because of this effect, also its frequency of approximately $500\ \mathrm{s}^{-1}$ was investigated.

4.3 Analysis

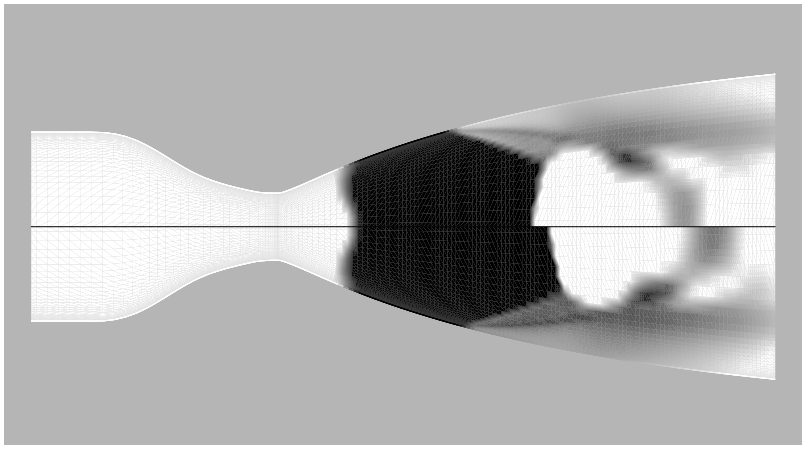

Figure 17. Pressure field at $\omega = 1500\ \mathrm{s}^{-1}$. Top: unsteady case at the extreme shock position. Bottom: steady case.

The evaluation of the results presented in this work focuses on a detailed investigation of the estimated sideloads and the movement of the oblique shock on the nozzle wall. The general flow field was already discussed in the previous chapter and the results for the considered frequencies did throughout all the runs not show any differences compared to the character of the flow as presented in chapter 3. Nevertheless, figure 17 shows as an example a flow situation with maximal deflection of the shock away from the steady solution. The fluctuation of the pressure on the wall can be seen in the unsteady flow field and the statement about the unchanged character of the flow is confirmed. The amplitude of the shock movement corresponds well to what is expected from the steady solutions.

Figure 18 presents the pressure fluctuations in the three different evaluation points, that are visualized in figure 14. Those points were chosen to impart a picture of how the external disturbance is carried into the nozzle towards the wall shock. The first point is located right on the external boundary close to the exit and its pressure values show the effective fluctuations due to the interpolation of the Riemann condition between freestream and computational domain. The second point is located in the inflowing region of the recirculation area and the third one in the shear layer that separates supersonic jet and recirculation area, rather close to the origin of the oblique shock. With the help of these three points the propagation of fluctuations through the region close to the wall can be followed quite accurately.

It can be stated that for all considered frequencies the fluctuations easily reach the shock, but obviously a phase shift occurs that increases with the frequency. The phase shift corresponds well to the propagation of the fluctuations with sound velocity, which also can be shown. A closer comparison of the relation between the pressure fluctuations in the two inner evaluation points and the freestream pressure fluctuation (figures 19 and 20) illustrates how the phase shift increases gradually while the fluctuation propagates into the nozzle towards the shock.

Figure 18. Pressure history in the three evaluation points of figure 14.

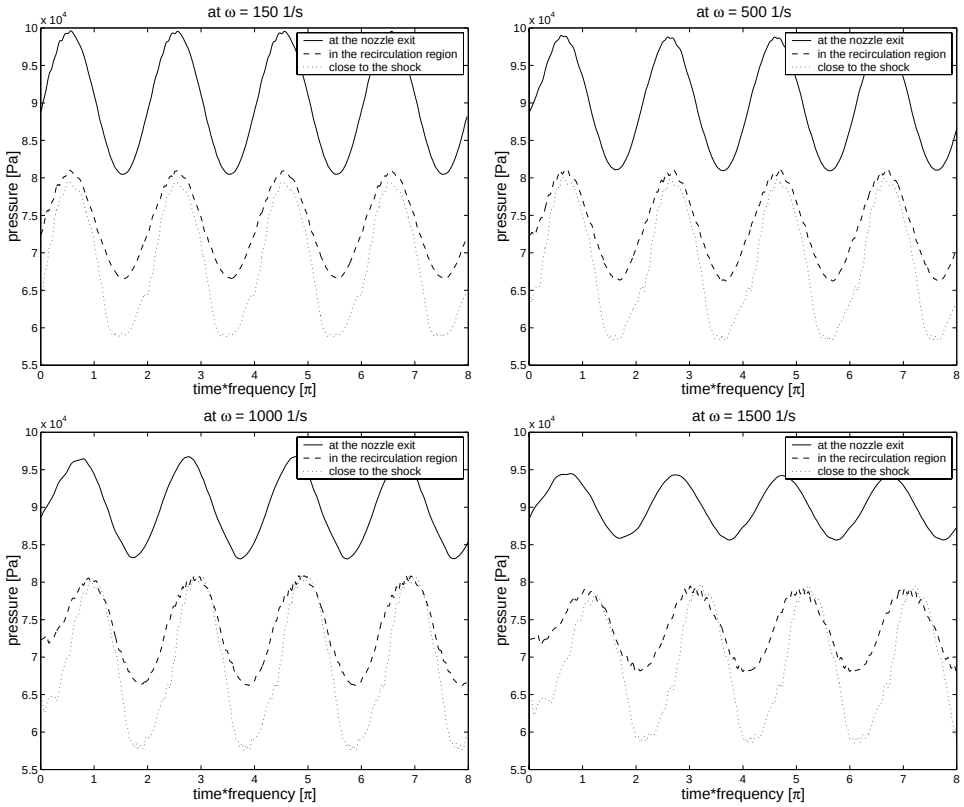

Figure 19. The pressure in the recirculation area (point 2 in figure 14).

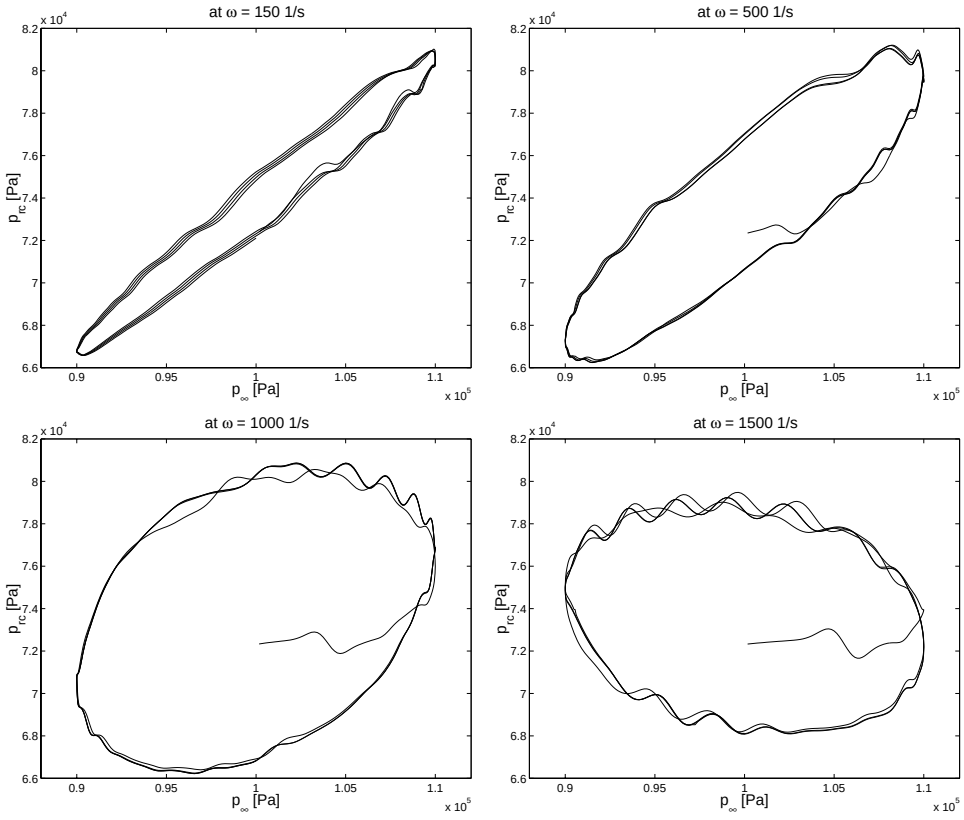

It is remarkable, though, that the amplitude of the pressure fluctuations at the exit goes down considerably with frequency, but stays approximately

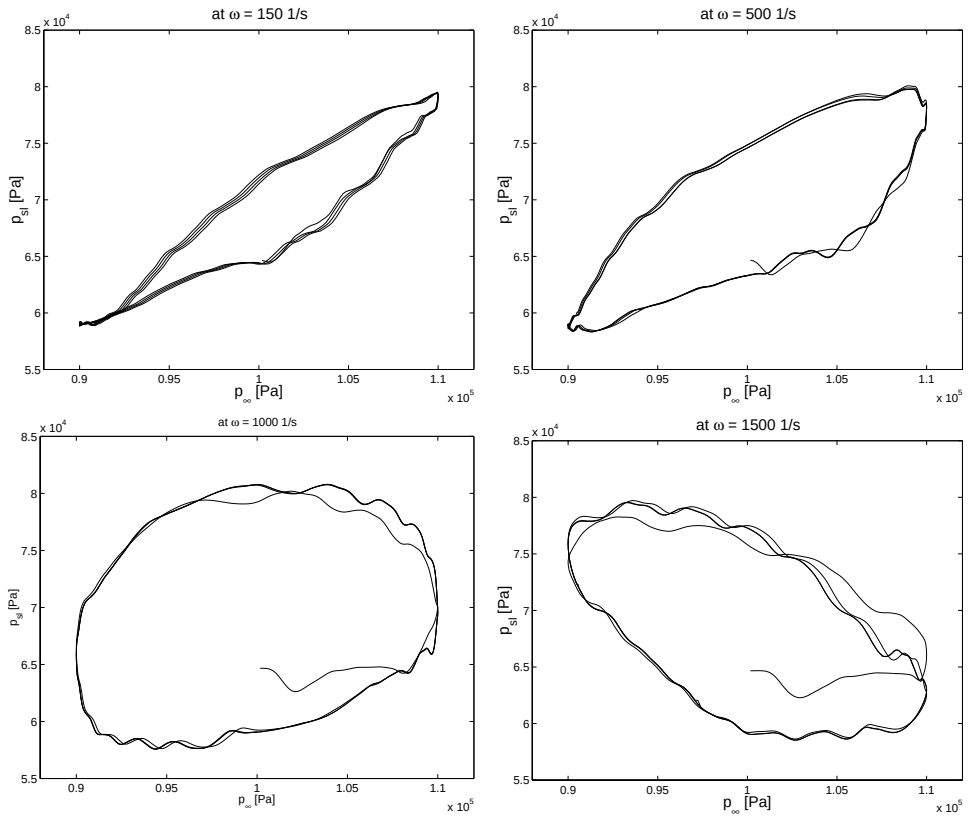

Figure 20. The pressure in the shear layer (point 3 in figure 14).

the same close to the shock. Figure 16 shows, that the radial velocity at the exit rises, so that the total pressure amplitude can be expected to be similar for the different frequencies. Another noticeable effect is the appearance of small oscillations, that are overlaid on the overall fluctuations at the two inner points independent of the frequency. It will be discussed in the next section, how these effects relate to the shock movement. However, the reason for the fluctuations in the velocity field (see figure 16) remains unclear.

4.3.1 Movement of the Shock Structure

In this section the reaction of the shock on the imposed fluctuations is investigated. Also the interaction between fluctuation propagation and shock movement is analyzed. For this purpose, the wall solution was interpolated on a finer resolution of wall points. Then, the shock position was determined from this solutions simply by evaluating the pressure gradients on the wall.

A look on figure 21 shows, that in the computations the movement of the shock on the wall occurs in steps. It is clearly visible how the shock is moved not continuously, but cell wise through the mesh. It is locked to one cell for several time steps and jumps then on to the next cell. A comparison between the time it is locked in one cell and a period of the small oscillations in pressure mentioned in the last section suggests that

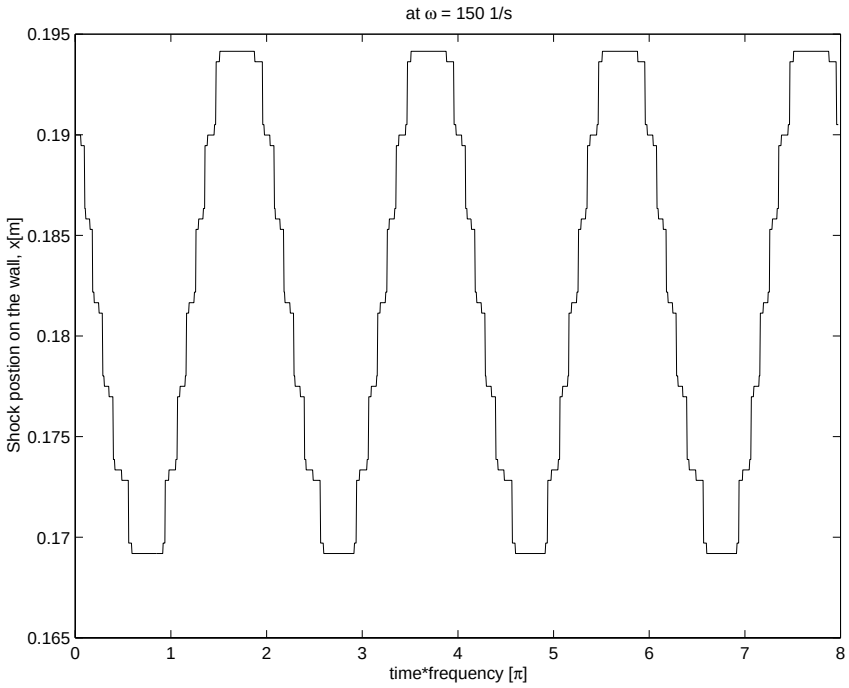

Figure 21. The oblique shock movement on the wall.

these oscillations are caused by the stepwise shock movement. This is confirmed by the fact, that both the oscillations and the stepwise movement appear independently of frequency and timestep and keep the same relation to the fluctuation's period. The stepwise movement of the shock might be resolved by refining the mesh. However, the mesh would have to be refined by at least a factor of eight, which leads to an impractically huge mesh.

For the sake of convenience for the reader the shock movement was smoothed by a fitting using 21st-order-polynomials throughout the following analysis.

The phase shift that is observed in the pressure history can also be observed in the shock movement (figure 23). The phase of the shock movement is, with increasing frequency, shifted more and more, up to half a period for $1500\ \mathrm{s}^{-1}$, compared to the pressure fluctuation. Considerable hysteresis effects occur. However, the steady state solution lies well positioned in the center of the unsteady shock movement (figure 22), so that the solutions of the steady and unsteady case can be considered consistent, and the choice of the steady forces as mean forces for the sideloads is justified (see 4.3.2).

The shock positions compared to the pressure in the shear layer are not shifted in phase and the picture looks similar for all investigated frequencies. Also the range, in which the shock moves, is exactly the same for all four frequencies. Furthermore, the occurring phase shift corresponds well to a propagation of the fluctuation with freestream sound velocity into the nozzle. Thus, it can be concluded, that the phase shifts that appear in this analysis are probably all due to the propagation of the fluctuation through the low speed separated region, and are not a consequence of a delayed reaction of the shock.

Figure 22. The movement of the oblique shock on the wall, the crosses mark the results from the steady case (compare figure 7).

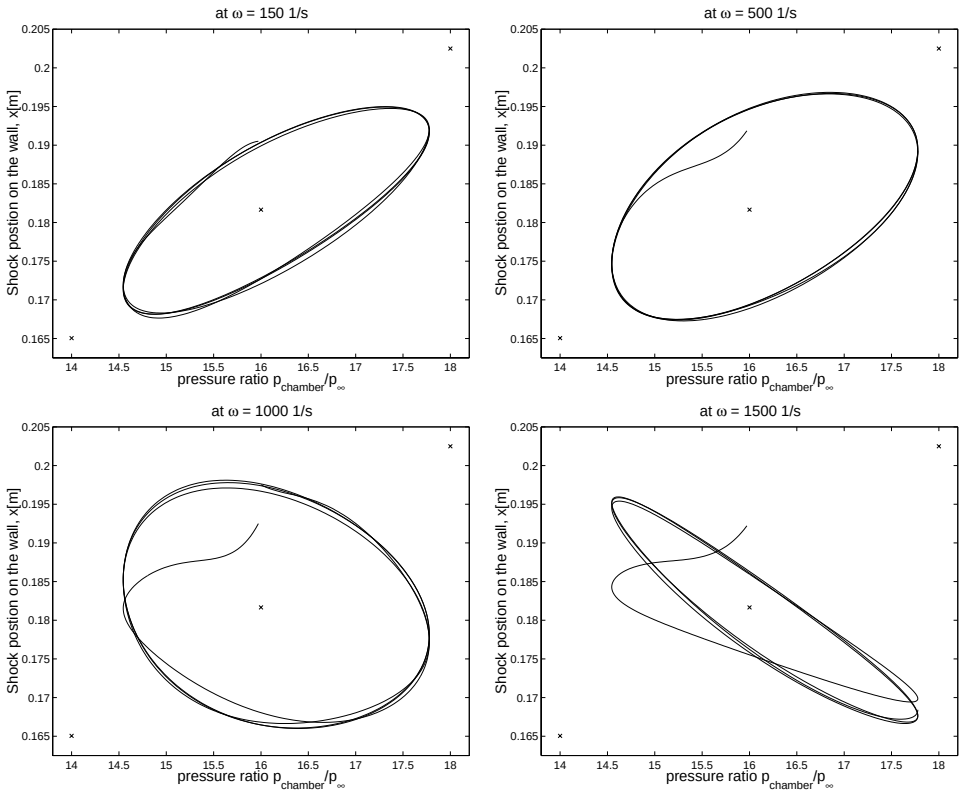

Figure 23. The wall shock movement compared to the freestream pressure.

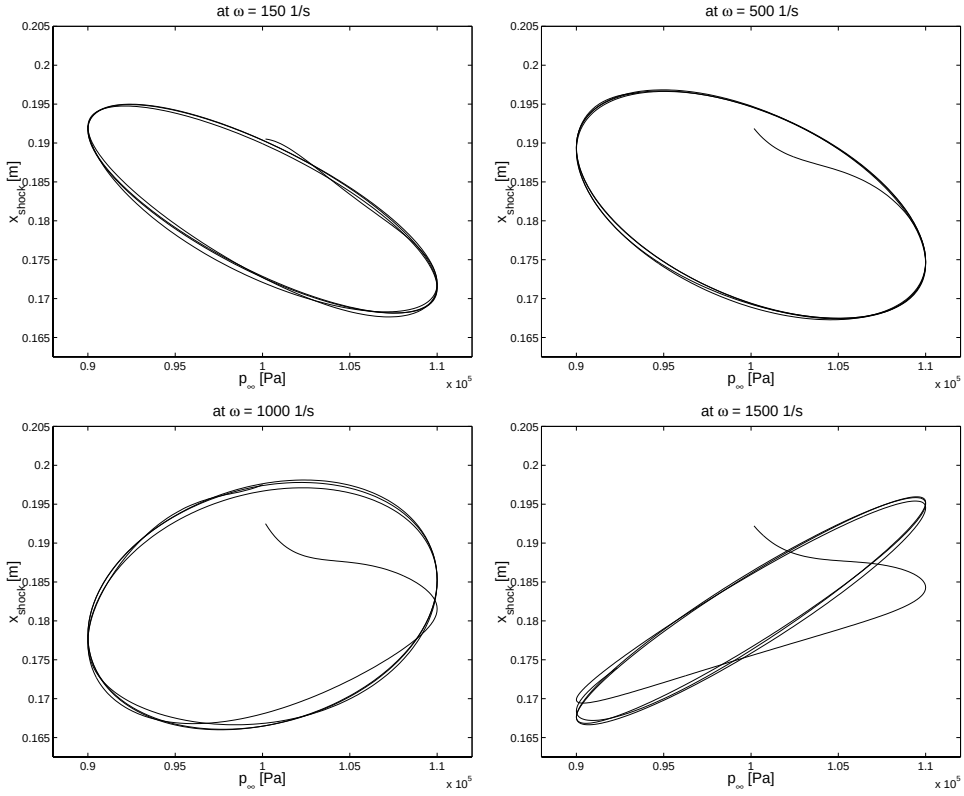

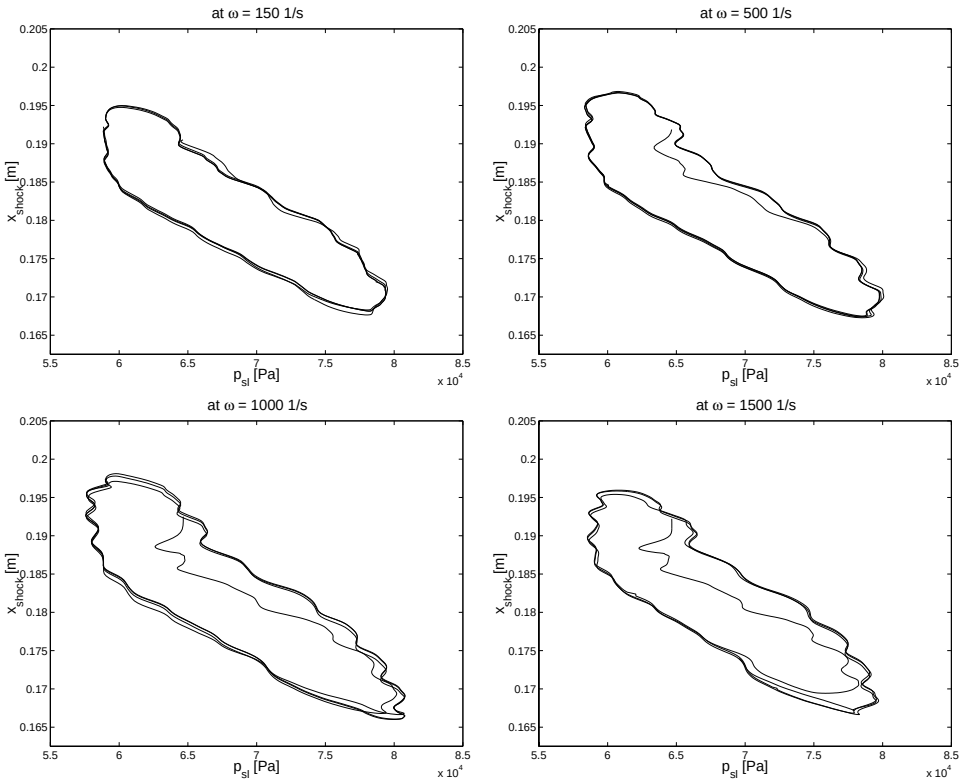

Figure 24. The wall shock movement compared to the pressure in the shear layer (point 3, figure 14).

4.3.2 Sideloads

To estimate sideloads, an axisymmetric approximation has to be defined, that maintains the asymmetric character of this phenomenon.

The general force on the nozzle body is given by

$$F = \oint_{wall} p(\underline{x}, t) \mathrm{d}\underline{A} \quad , \tag{15}$$

where x is the coordinate along the nozzle axis.

The component of the force that acts on a radial intersection from nozzle throat to nozzle exit generated by the inner pressure distribution is then

$$\mathrm{d}F_i = \int_{throat}^{exit} p(x,t) r(x) \mathrm{d}x \quad , \tag{16}$$

with $r(x)$ for the distance from the nozzle axis to the wall.

As the ambience of the nozzle is not part of the computational domain in this work, it has to be estimated in some way. Here the freestream pressure at the Riemann boundary condition is chosen to act on the whole nozzle length:

$$\mathrm{d}F_\infty = \int_{throat}^{exit} p_\infty(t) r(x) \mathrm{d}x \quad . \tag{17}$$

Sideloads are, as mentioned in section 2.1, caused by asymmetries of the, in reality, three-dimensional flow field. Nevertheless, if the fluctuations of the intersections are regarded as independent of each other, the

radial load caused by one of these fluctuations can be estimated by comparison of the force $\mathrm{d}F$ that it generates, compared to some mean force $\mathrm{d}F_0$, which in this case can be given from the steady case. Thus, an estimation of the sideloads can be formulated with

$$\mathrm{d}S_i = \frac{\mathrm{d}F_i(t) - \mathrm{d}F_{0,i}}{\|\mathrm{d}F_{0,\infty}\|} \tag{18}$$

for the inner sideload,

$$\mathrm{d}S_\infty = \frac{\mathrm{d}F_\infty(t) - \mathrm{d}F_{0,\infty}}{\|\mathrm{d}F_{0,\infty}\|} \tag{19}$$

for the outer sideload and

$$\mathrm{d}S_{tot} = \frac{\mathrm{d}F_{tot}(t) - \mathrm{d}F_{0,tot}}{\|\mathrm{d}F_{0,\infty}\|} \tag{20}$$

for the total sideload $\mathrm{d}S_{tot} = \mathrm{d}S_i - \mathrm{d}S_\infty$. However, these are only rough estimations, as only single modes of the mechanisms that generate sideloads are covered by this model.

The above sideloads defined for this case can be expected to be affected by basically two interacting processes: the propagation of the fluctuation into the nozzle will cause deviations from the mean wall pressure level behind the oblique shock while the shock itself moves the pressure jump on the wall up- and downstream, as illustrated in figures 25 and 26.

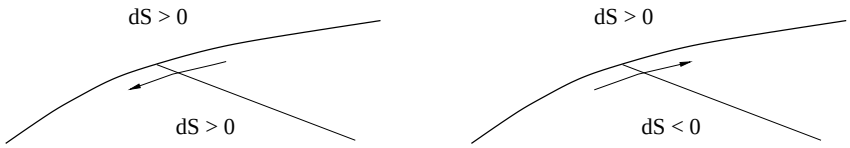

Figure 25. Sideload generation due to shock movement. Left : in phase. Right: out of phase.

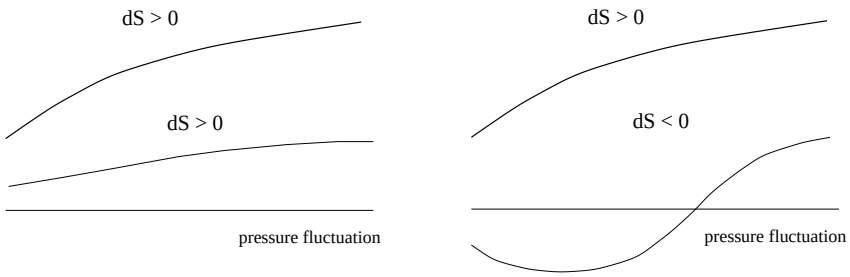

Figure 26. Sideload generation due to fluctuation propagation. Left: in phase. Right: out of phase.

Figure 27 reveals that with increasing frequency the inner sideload starts to fall behind the imposed fluctuation, so that at 1500 s^{-1} the phase shift between inner and outer sideload reaches little less than half a period. This has severe effects on the total sideload, as can be seen in figure 28. While the total sideload does not exceed 2.5 % of the mean outer force on the intersection while in phase, it reaches more than 13 % when the phase shift reaches half a period. This phase shift occurs due to the time lag in fluctuating pressure on the nozzle inside and in the moving of the shock, caused by the delayed propagation.

Figure 27. Inner and outer sideloads.

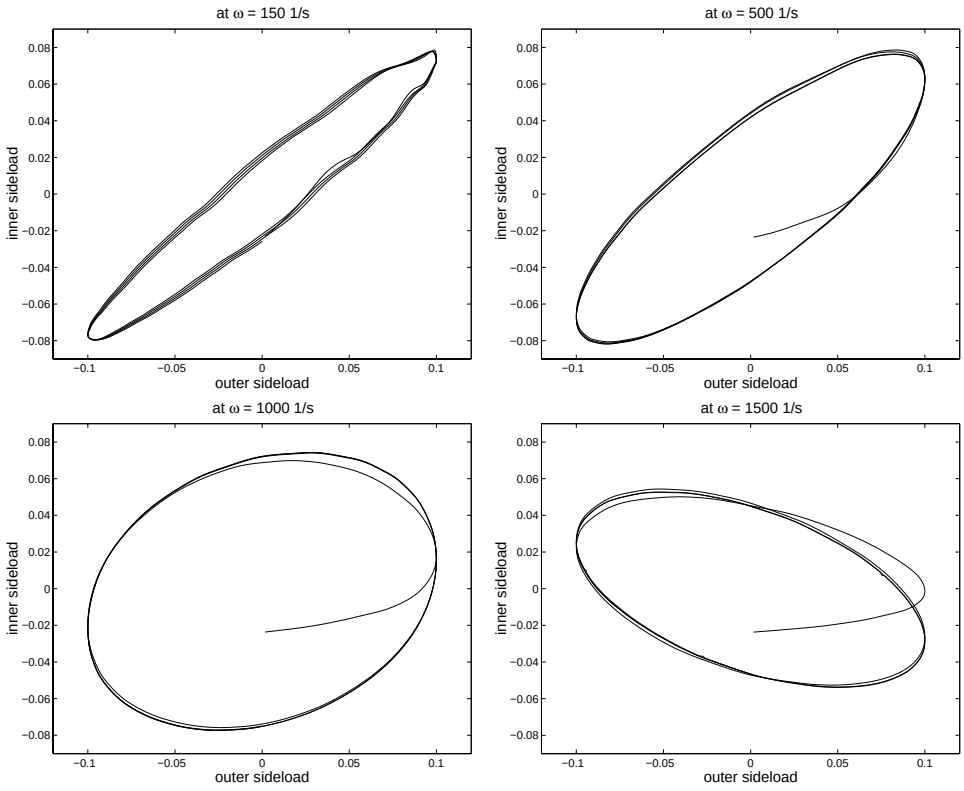

Figure 28. Sideloads for different frequencies.

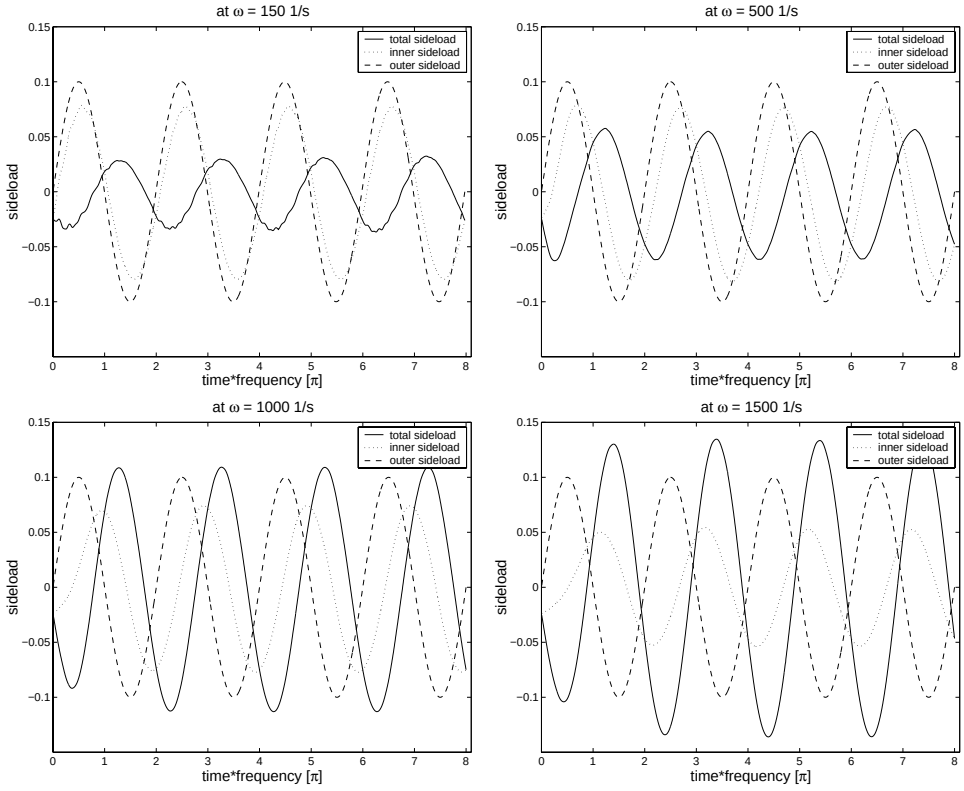

5 Conclusions

The presented work could, though in itself axisymmetric, present a number of expected and unexpected effects and results about the unsteady and asymmetric behavior of overexpanded nozzle flow. The steady analysis presents a variety of results that agree well with observations previously done by other authors and, thus, providing a solid base for the unsteady analysis.

The flow structure of the steady solutions was preserved in the unsteady case. It is shown that the imposed periodic fluctuations in pressure were propagating continuously into the nozzle and reached the wall shock to full extend.

For the investigated frequency spectrum, the oscillation of the shock was taking place in a constant range along the nozzle wall, while the phase shift observed at the higher frequencies was found to be related to the propagation of the pressure signal. A delayed reaction of the shock itself was not found.

The propagating pressure fluctuation and the phase shift between signal and shock movement was shown to create heavy side loads for increasing frequency.

It would surely be interesting to investigate the case for further increased frequencies. One could then expect that the wall shock is even more lagging behind the ambient pressure fluctuations and that the effect of the fluctuations on the inner sideload decreases. A more general investigation of the numerics of shock movement due to ambience fluctuations could be helpful as well.

Furthermore, only a full 3D analysis will give a complete picture of the modes that excite the shock movement and the sideloads, taking their interactions into account.

Also a direct validation of the numerical solutions with the help of experimental results would be helpful. Especially for assessing the appropriate turbulence model.

6 Acknowledgments

A lot of people supported me in the realization of this work and contributed to it.

I would like to thank the FOI/Sweden that hosted me for the duration this work, i.e. the complete stuff of the department for computational aerodynamics for their hospitality and help. Special thanks to Ingemar Lindblad who introduced me to the subject of this work and invited me to the FOI, Jan Nordström and Gunilla Efraimsson who gave a lot of helpful advises and Peter Eliasson who helped with all questions concerning the Navier Stokes solver, but most of all to Stefan Wallin and Mattias Chevalier who supported me continuously and intensively throughout the work and thus, contributed considerably to its outcome. Last but not least I would like to thank Arne Johansson at the KTH Stockholm for the supervision of the work.

Financial support from FOI is gratefully acknowledged.

References

[1] J. Boussinesq. Théorie de l'écoulement tourbillant. *Présentés par Divers Savants Acad. Sci. Inst. Fr.*, 23, 1877.

[2] C. L. Chen, S. R. Chakravarthy, and C. M. Hung. Numerical investigation of separated nozzle flow. *AIAA Journal*, 32(9), 1994.

[3] T. Damgaard. Personal communication. Volvo Aero Corporation, Trollhättan, Sweden.

[4] G. E. Dumnov. Unsteady side-loads acting on the nozzle with developed seperation zone. *AIAA Paper 1996-3220*, july 1996.

[5] P. Eliasson and J. Nordström. The developement of an unsteady solver for moving meshes. *FFA TN 1995-39*, 1995.

[6] M. Frey and G. Hagemann. Status of flow separation prediction in rocket nozzles. *AIAA Paper 98-3619*, july 1998.

[7] M. Frey and G. Hagemann. Flow seperation and side-loads in rocket nozzles. *AIAA Paper 99-2815*, june 1999.

[8] G. Hagemann, H. Immich, Thong Van Nguyen, and Dumnov G. E. Advanced rocket nozzles. *Journal Of Propulsion and Power*, 14(5), 1998.

[9] A. Jameson. Time dependent calculations using multigrid, with applications to unsteady flows past airfoils and wings. *AIAA Paper 91-1596*, 1991.

[10] C. Lacor, Z. W. Zhu, and C. Hirsch. A new family of limiters within the multigrid/multiblock navier-stokes code euranus. *AIAA/DGLR 5th Int. Aerospace Planes and Hypersonics Conf., Munich*, 1993.

[11] Ingemar Lindblad and Momme Butenschön. CFD analysis of the GSTP external expansion nozzle. Technical Report FFA-B-108, FFA, Sweden, 1999. Rev. 1.

[12] F. R. Menter. Two-equation eddy-viscosity turbulence models for engineering applications. *AIAA Journal*, 32(8), August 1994.

[13] M. Onofri and F. Nasuti. The physical origins of side loads in rocket nozzles. *AIAA Paper 99-2587*, june 1999.

[14] J. Östlund and M. Jaran. Assessment of turbulence models in over-expanded rocket nozzle flow simulations. *AIAA Paper 99-2583*, june 1999.

[15] Rizzi, A., Eliasson, P., Lindblad, I., Hirsch, C., Lacor, C., and Hauser, J. The engineering of multiblock/ multigrid software for navier-stokes flows on structured meshes. *Computers Fluids*, 31:341–367, 1993.

[16] G. L. Romine. Nozzle flow separation. *AIAA Journal*, 36(9), 1998.

[17] L. Tysell and S. G. Hedman. Towards a general threedimensional grid generation system. *ICAS Paper 88-4.7.4*, 1988.

[18] S. Wallin and A. V. Johansson. An explicit algebraic reynolds stress model for incompressible and compressible turbulent flows. *Journal of Fluid Mechanics*, 403:89–132, 2000.

[19] Dieqian Wang, Stefan Wallin, Martin Berggren, and Peter Eliasson. A computational study of unsteady turbulent buffet aerodynamics. *AIAA Paper 2000-2657*, 2000.

[20] D. C. Wilcox. *Turbulence Modeling for CFD*. DCW Industries, 2nd edition, 1998.

Issuing organisation	Report number, ISRN	Report type
FOI – Swedish Defence Research Agency Division of Aeronautics, FFA SE-172 90 STOCKHOLM	FOI-R–0173–SE	Scientific report
	Month year October 2001	Project number E840313
	Customers code 3. Aeronautical Research	
	Research area code 7. Vehicles	
	Sub area code 73. Aeronautical Research	

Author(s)	Project manager
Momme Butenschön	Stefan Wallin
	Approved by Torsten Berglind Head, Computational Aerodynamics Department
	Scientifically and technically responsible Stefan Wallin

Report title

Numerical Analysis of Time Dependent External Disturbances on Separated Axisymmetric Nozzle Flow

Abstract

In overexpanded rocket nozzle flow at low altitudes, the sensitivity of the shock structure, that develops inside the expansion part of the nozzle, causes severe problems in modern nozzle design. This shock structure is highly unstable, so that small fluctuations in the flow field can lead to heavy asymmetric loads on the nozzle. The movement of the shock structure is analyzed numerically by imposing a periodically fluctuating pressure to an external boundary face. The effects on the sideloads are estimated by an usteady axisymmetric analysis. The unsteady analysis shows, for the investigated frequency range, how the fluctuation propagates, the shock movement develops and sideloads are generated.

Keywords

rocket nozzle, separated flow, time-dependent flow, turbulent flow

Further bibliographic information

ISSN	Pages	Language
ISSN 1650-1942	47	English
	Price Acc. to price list	
	Security classification OPEN	

Utgivare	Rapportnummer, ISRN	Klassificering
Totalförsvarets Forskningsinstitut – FOI Avdelningen för Flygteknik, FFA SE-172 90 STOCKHOLM	FOI-R–0173–SE	Vetenskaplig rapport
	Månad år Oktober 2001	Projektnummer E840313
	Verksamhetsgren 3. Flygteknisk forskning	
	Forskningsområde 7. Bemannade och obemannade farkoster	
	Delområde 73. Flygteknisk forskning	

Författare	Projektledare
Momme Butenschön	Stefan Wallin
	Godkänd av Torsten Berglind Chef, Institutionen för beräkningsaerodynamik
	Tekniskt och/eller vetenskapligt ansvarig Stefan Wallin

Rapporttitel

Numerisk analys av tidsberoende yttre störningar på separerad strömning i axisymmetriska dysor

Sammanfattning

Ett stort problem vid design av moderna raketmunstycken är att stötmönstret som bildas vid överexpanderat tillstånd är känsligt för yttre störningar. Stötmönstret är mycket instabilt, vilket innebär att små störningar i strömningsfältet kan ge stora asymmetriska laster på munstycket. Stötens rörelser har analyserats numeriskt genom att ansätta en periodisk tryckfluktuation på den yttre beräkningsranden. Sidolasterna har uppskattats från en tidsberoende axisymmetrisk analys. Inom det frekvensområde som studerats, visar den tidsberoende analysen hur störningarna propagerar, stötrörelserna utvecklas samt hur sidolasterna genereras.

Nyckelord

raketmunstycke, separerad strömning, tidsberoende strömning, turbulent strömning

Övriga bibliografiska uppgifter

ISSN	Antal sidor	Språk
ISSN 1650-1942	47	Engelska
Distribution enligt missiv	Pris Enligt prislista	
	Sekretess ÖPPEN	